Supplementary Material

Nanoflow Electrospinning Serial Femtosecond Crystallography

Raymond G. Sierra[1], Hartawan Laksmono[1], Jan Kern[2,3], Rosalie Tran[2], Johan Hattne[2], Roberto Alonso-Mori[3], Benedikt Lassalle-Kaiser[2], Carina Glöckner[4], Julia Hellmich[4], Donald W. Schafer[3], Nathaniel Echols[2], Richard J. Gildea[2], Ralf W. Grosse-Kunstleve[2], Jonas Sellberg[5,6], Trevor A. McQueen[7], Alan R. Fry[3], Marc M. Messerschmidt[3], Alan Miahnahri[3], M. Marvin Seibert[3], Christina Y. Hampton[1], Dmitri Starodub[1], N. Duane Loh[1], Dimosthenis Sokaras[5], Tsu-Chien Weng[5], Petrus H. Zwart[2], Pieter Glatzel[8], Despina Milathianaki[3], William E. White[3], Paul D. Adams[2], Garth J. Williams[3], Sébastien Boutet[3], Athina Zouni[4], Johannes Messinger[9], Nicholas K. Sauter[2], Uwe Bergmann[3], Junko Yano[2], Vittal K. Yachandra[2], Michael J. Bogan[1,3*]

[1] PULSE Institute, SLAC National Accelerator Laboratory, Menlo Park, CA 94025, USA
[2] Physical Biosciences Division, Lawrence Berkeley National Laboratory, Berkeley, CA 94720, USA
[3] LCLS, SLAC National Accelerator Laboratory, Menlo Park, CA 94025, USA
[4] Max-Volmer-Laboratorium für Biophysikalische Chemie, Strasse des 17 Juni 135, Technische Universität Berlin, D-10623 Berlin, Germany
[5] SSRL, SLAC National Accelerator Laboratory, Menlo Park, CA 94025, USA
[6] Department of Physics, AlbaNova, Stockholm University, S-106 91 Stockholm, Sweden
[7] Department of Chemistry, Stanford University, Stanford, CA 94025, USA
[8] European Synchrotron Radiation Facility, Grenoble Cedex, France
[9] Institutionen för Kemi, Kemiskt Biologiskt Centrum, Umeå Universitet, Umeå, Sweden

[*] To whom correspondence should be addressed.
Correspondence e-mail: mbogan@slac.stanford.edu

Supplementary Methods: Electrospinning nanoflow SFX at CXI:
One of the challenges to overcome in the use of the electrospun jet is that LCLS SFX is performed at $<10^{-4}$ mbar in order to minimize background scattering. This pressure regime is outside of the typical atmospheric pressure operation of electrosprays so heaters must be used to start the electrospray of water in vacuum. However, electrospray of pure glycerol is known to be stable at <0.01 mbar and no heater is required. Conveniently, glycerol is also commonly used in crystal screens and as a cryoprotectant in synchrotron protein crystallography. We observed that glycerol solutions 25-40% weight/volume (w/v) produced stable electrosprays at $<10^{-4}$ mbar. Similar to electrospray of solutions of pure glycerol, electrospun jets of crystal suspensions showed highest stability at pressures below 0.01 mbar, outside the corona discharge regime.

A 100 µl aliquot of the sample (see Supplementary Figure 4) in a microcentrifuge tube was loaded into the pressurized cell that established fluid communication with a 114 cm long, 50 µm ID x 150 µm OD silica capillary and a platinum electrode (Supplementary Fig. 1). The capillary delivered the sample to the interaction region inside the vacuum chamber through a 1/16" Swagelok fitting and an 180µm adapter sleeve. The capillary length is set by the large diameter of the CXI endstation vacuum chamber. An inlet port closer to the X-ray interaction region would permit for smaller capillary lengths. The current setup can accommodate up to 8 different capillaries simultaneously installed in the vacuum chamber. Typical operation utilizes 3 capillaries mounted inside the vacuum chamber at one time to provide redundancy in case of capillary clogging or other failure.

By using only one continuous capillary the potential of clogging at tubing and capillary unions is minimized, allowing the delivery of crystals of relatively large sizes compared to the inner diameter of the capillary. For example in the PS II experiment[22] it was possible to deliver crystals with maximum dimensions of up to 30 µm using a 100 µm ID capillary. In the case of larger ID (75 and 100 µm) and 360 µm OD tapering of the OD of the capillary at both ends was used. This minimized the potential for clogging of the crystals at the surface around the entrance of the capillary and enhanced jet formation at the exit of the capillary by minimizing wetting.

The capillary was attached to a stack of three XYZ nanopositioning stages inside the vacuum chamber for positioning relative to the X-rays (Supplementary Fig. 2). The counter electrode was an aluminum block with a 1 cm bore and was positioned 5-8 mm from the capillary exit. A +2.5 kV potential (Stanford Research Systems, PS350) was applied to the platinum electrode submersed in the sample vial and -0.2 kV (Stanford Research Systems, PS350) was applied to the counter electrode, resulting in electric fields between 3400- 5400 V/cm. The nanoflow liquid jet was visualized using the CXI microscope on-axis with the X-rays and was illuminated by a 532 nm nanosecond pulsed laser or a 785 nm CW laser (Supplementary Figure 3).

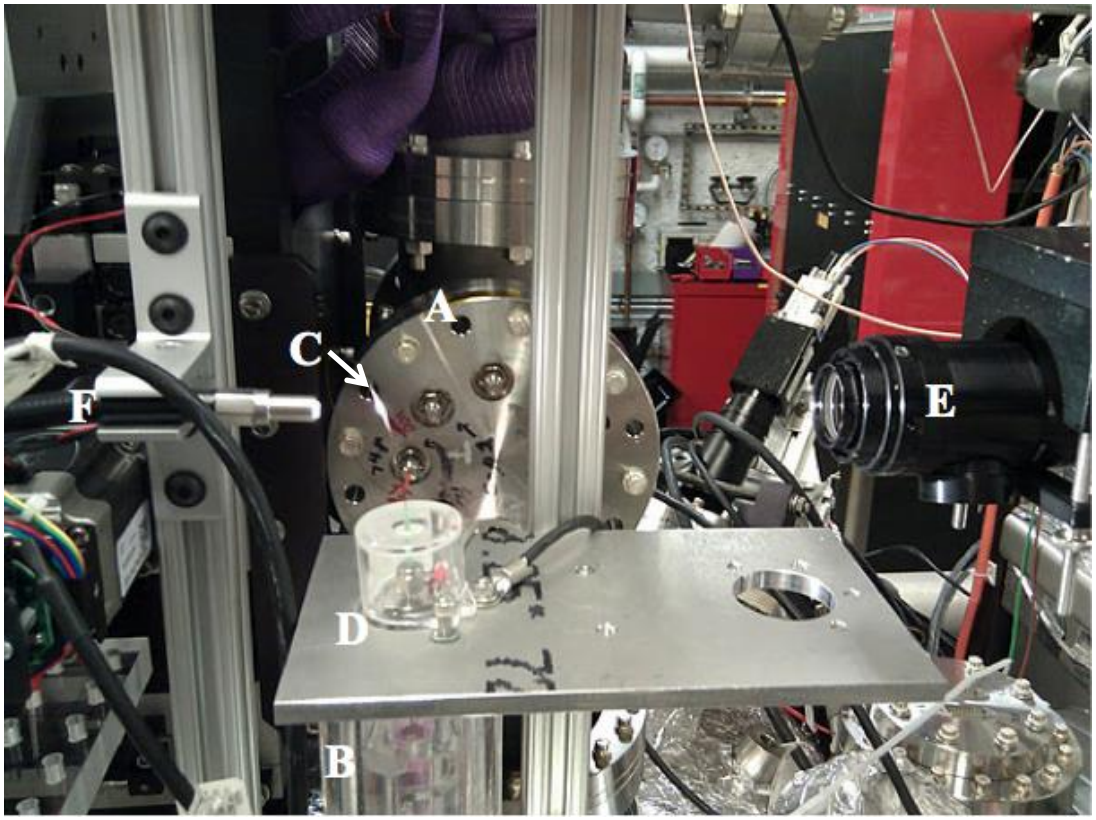

Supplementary Figure 1. Nanoflow electrospinning SFX experimental setup at the LCLS CXI endstation: sample introduction setup outside of the vacuum chamber. A) the feedthrough vacuum flange with eight 1/16" Swagelock + 180 μm sleeve feedthroughs, all unused ports are capped; B) the pressurized cell holding the microcentrifuge tube of sample (purple vial); C) the 50 μm ID x 50 μm OD coated, fused-silica capillary looping out of the pressure cell at *D* and into the vacuum chamber through *A*; D) the high voltage source (Stanford Research Systems PS350) is attached through this a proprietary Swagelock feedthrough (TSI) combined with a platinum electrode submersed in the reservoir, B, the high voltage source (Stanford Research Systems PS350) is attached through this proprietary piece ; E) optics attached to a CMOS camera (Firefly, Point Grey) to qualitatively visualize the flowing crystal suspension; F) the fiber optics light to illuminate the capillary.

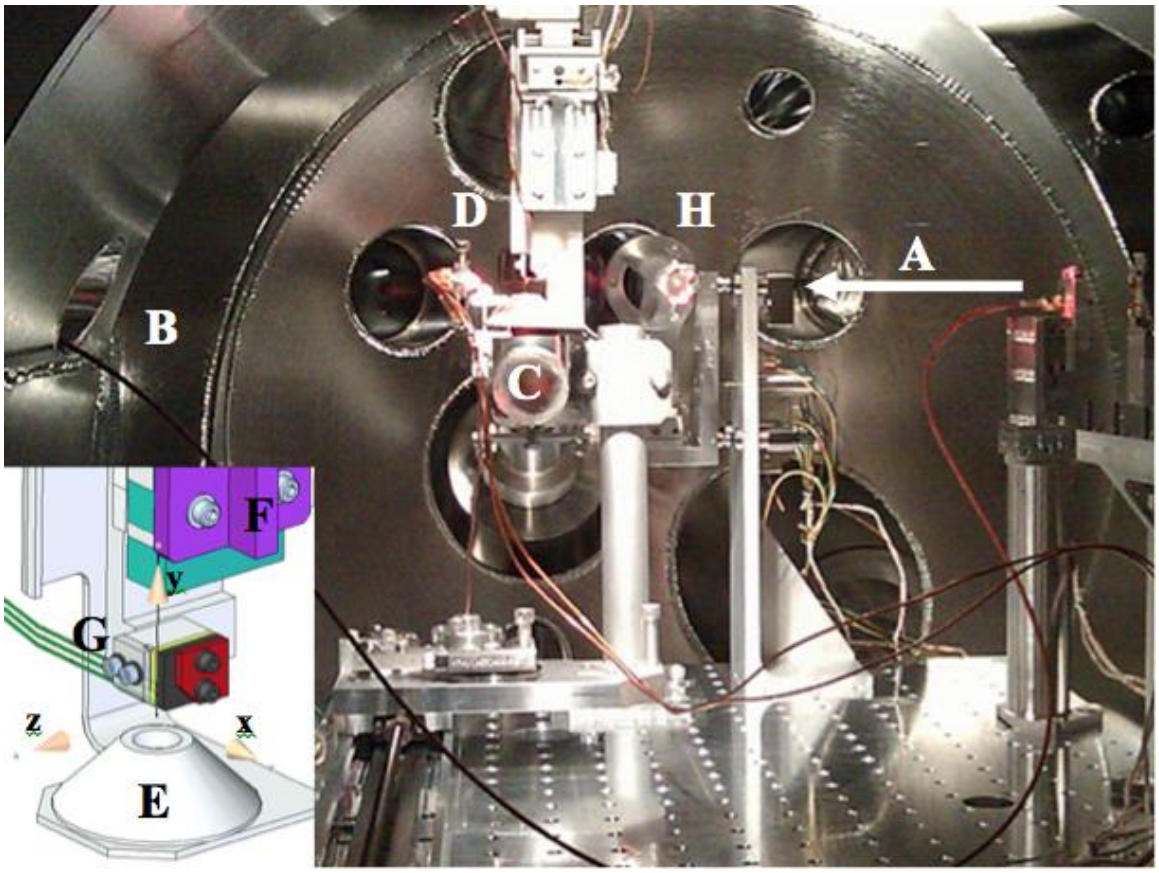

Supplementary Figure 2. Nanoflow electrospinning SFX experimental setup at LCLS CXI endstation: sample introduction setup inside the vacuum chamber. A) Direction of incident X-ray laser beam (coincides with the z-direction in the inset; B) location of the CSPAD detector (not shown); C) sample catcher connected to a turbopump in order to collect sample waste and prevent sample from contaminating the chamber; D) capillary mount (detailed CAD in the inset) with back-illuminating red LED; E) the aluminum sample catcher and counter electrode (CE) with 1 cm bore is tapered externally to allow for capture of diffraction at >65° with typical capillary-electrode separations of 5-8 mm; F) the Micos PP-30 stages allow for fine tuning of the capillary in the x, y, z direction in order to adjust the electric field and the position of the jet into the X-rays; G) three fiber optics attached to a custom mount to provide option to pump the sample for probing downstream by the X-ray (not utilized in this experiment); H) CXI optics for an on-axis camera which can visualize the jet as viewed by the X-ray laser, an optical laser (532 nm) (not seen here) or simple red LED can be used to illuminate the beam. The liquid exits the capillary at the origin of the coordinate axis and sprays downward into *E*. Excess fluid is collected in C. The 3 μm^2 focused X-ray laser passes between the capillary and the counter electrode. The 2-D diffraction pattern created in the x-y plane propagates along z towards the detector, B (not shown).

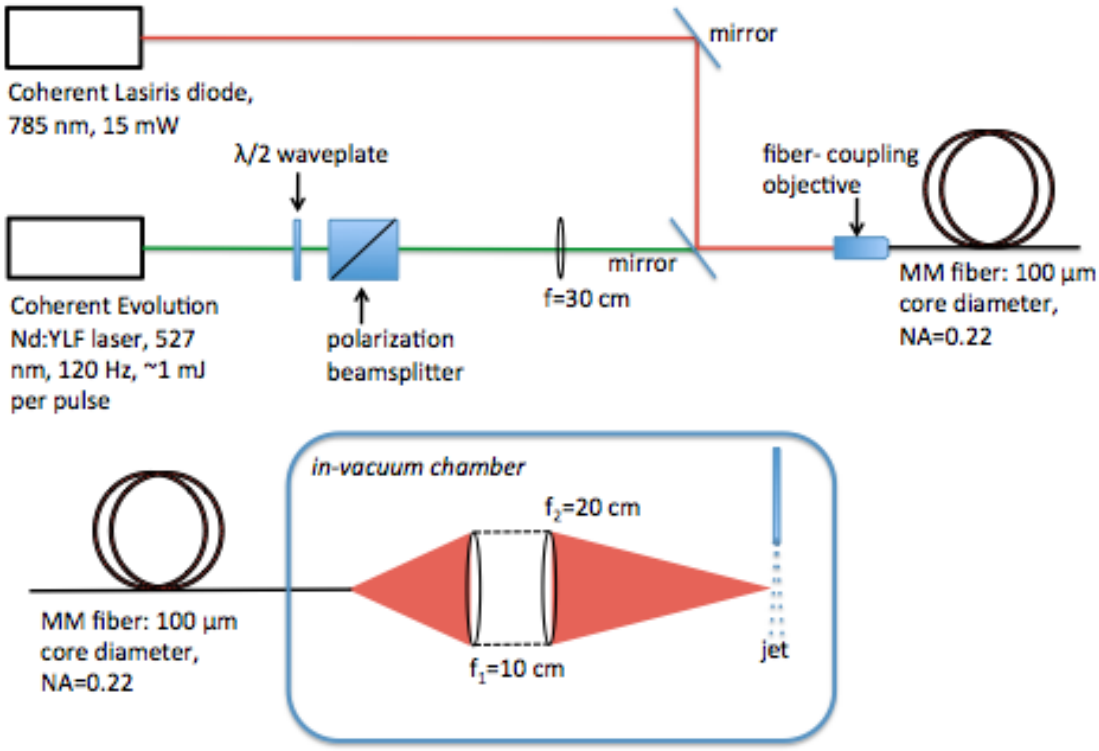

Supplementary Figure 3. Laser setup for illumination of jet inside CXI vacuum chamber.

Supplementary Table 1. Flow rates for electrospinning in vacuo in different capillaries.

ΔP (Psi)	Flow time (min)	Measured mass consumed (mg)	Calculated volume consumed (μl)	Flow rate (μl/min)
50 μm ID 114 cm long capillary				
15.7	60	9.34	8.45	0.14
16.7	60	10.58	9.58	0.16
17.7	60	11.06	10.01	0.17
18.7	60	12.12	10.96	0.18
19.7	60	12.64	11.44	0.19
75 μm ID 110 cm long capillary				
15.7	73	63.70	57.7	0.79
16.7	60	55.48	50.2	0.84
17.7	60	60.33	54.6	0.91
19.7	60	79.03	71.5	1.19
100 μm ID 120 cm long capillary				
15.7	60	166.44	150.7	2.51
16.7	60	190.37	172.3	2.87
17.7	60	195.08	176.6	2.94
19.7	60	207.00	187.4	3.12

Microjet flow rate measurements: The flow rate in our setup depends on the liquid viscosity, the pressure difference between the liquid reservoir and the vacuum chamber (ΔP), and the length and ID of the capillaries used. Thus, for a set of liquid solution, ΔP, and capillary length and ID, we determine the flow rates by measuring the mass of the liquid consumed for a certain amount of time, typically 1 hour, and dividing it by the density of the liquid solution used. We measure the density by weighing a known volume of liquid drop, typically 100μl, prepared using a pipette. We determined the density of the 30% Glycerol, 10% PEG 2000, 5mM $CaCl_2$, and 100mM MES buffer solution to be 1104±27 mg/ml. We determined the liquid flow rates of the buffer solution for 50, 75 and 100 um ID capillaries 114, 100 and 120 cm long, respectively, with ΔP varied from 15.7 to 19.7 Psi, and are summarized in Supplementary Table 1.

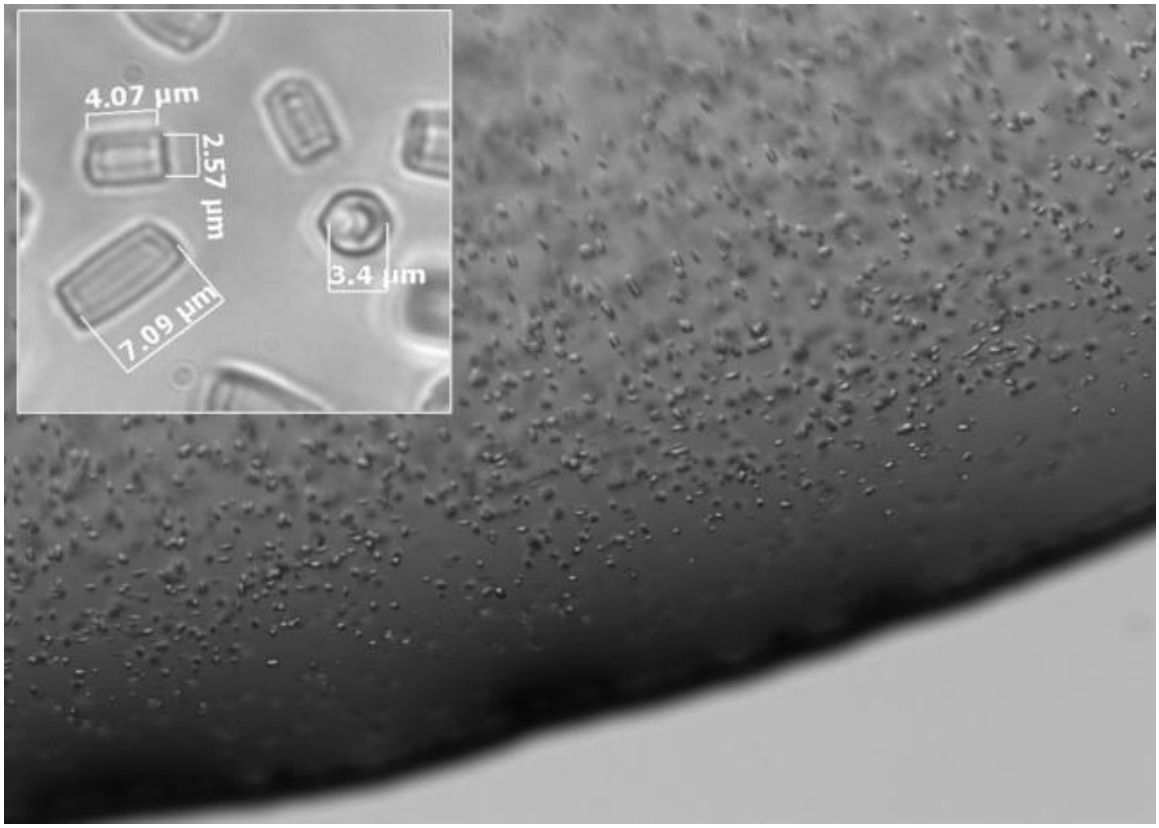

Supplementary Figure 4. Microscope images of a filtered thermolysin crystal suspension. Lyophilized thermolysin (Hampton Research) from *Bacillus stearothermophilus* was resuspended into a 25mg/mL protein crystallization stock solution in 0.05M NaOH. A suspension of thermolysin microcrystals was prepared by adding a 1:1 ratio of this stock solution with crystallization buffer containing 40% weight/volume (w/v) polyethylene glycol (PEG) 2000, 100mM MES pH 6.5. The microcrystals were then exchanged stepwise into buffer containing 30% (w/v) glycerol, with 10% (w/v) PEG2000, 100 mM MES, pH 6.5, 5 mM $CaCl_2$, dissolved in deionized water immediately prior to analysis. The crystals were then filtered through an 8 µm pore Nucleopore membrane (Whatman). On average the thermolysin crystals were 2x3x1 micron.

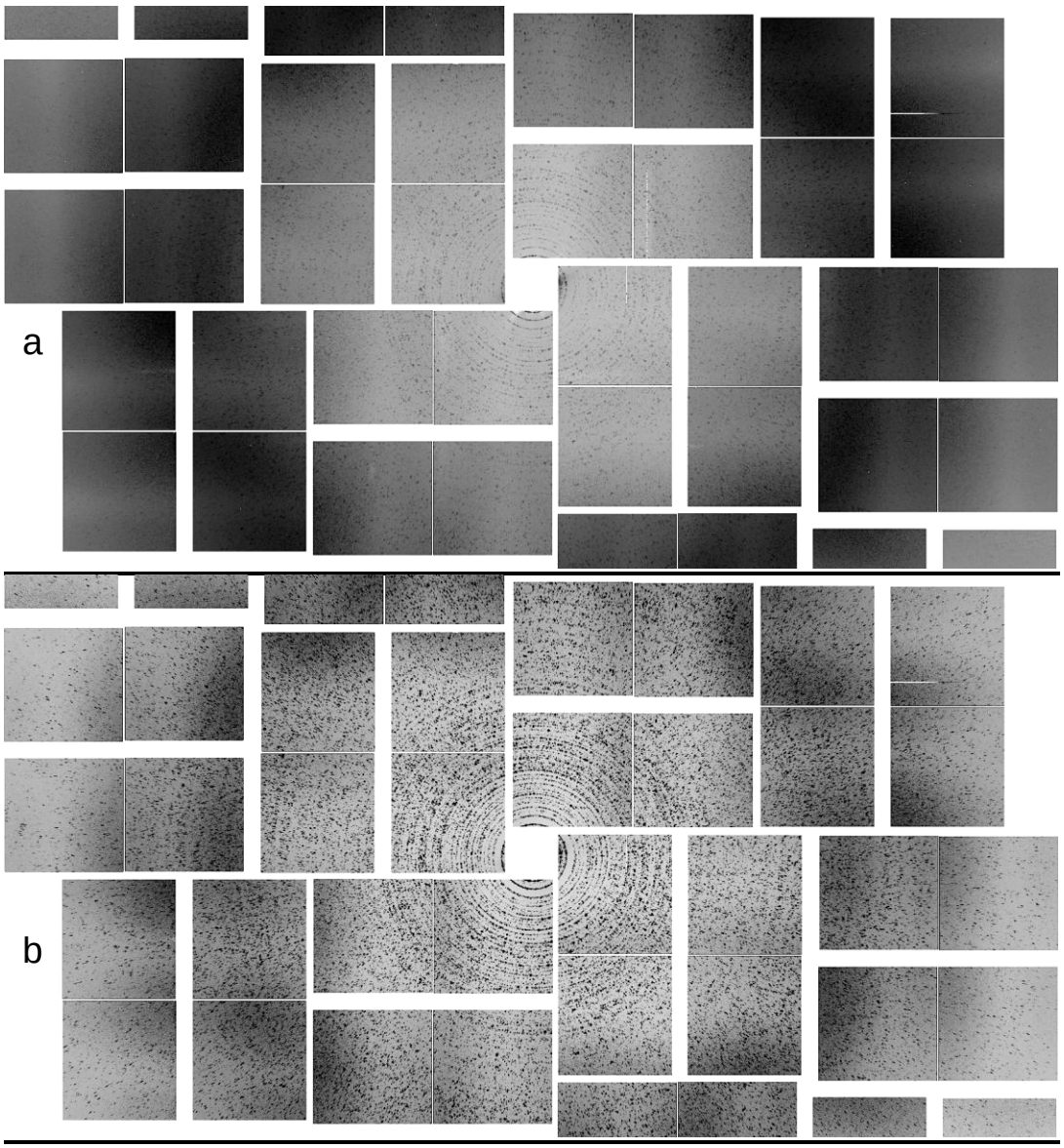

Supplementary Figure 5. Virtual powder pattern formed from serial femtosecond diffraction collected from an electrospun thermolysin crystal suspension. (a) Average of 1,024 indexable single-shot FEL diffraction patterns from <8 micron thermolysin crystals flowing at 170 nl/min in different orientations through the X-ray interaction region. **(b)** To enhance visualization, the pixel intensities in the image correspond to the sample standard deviation from 1,024 indexable diffraction images. A common background image, calculated as the average of 261,627 diffraction patterns without any discernible Bragg spots, was subtracted from each contributing diffraction pattern. The resolutions at the corners are approximately 4 Å. Details of the CSPAD detector have been published elsewhere[23,24]. The sample-detector distance was 175 mm. Single shot data where a crystal was hit giving rise to SFX diffraction patterns on the CSPAD were identified as those with ≥16 Bragg peaks using the software suite cctbx.xfel[22]. Detector geometry refinement, indexing and integration were also carried out using cctbx.xfel.

Supplementary Table 2. Typical operating parameters of microjets for SFX

Parameters	Gas dynamic virtual nozzle*	Electrospinning *in vacuo*
Flow focusing phenomenon	Gas	Electric field
Capillary Inner Diameter (ID)	10-100 μm	50, 75, 100 μm
Gas Sheath	15-1500 PSI	none
Liquid backing pressure	15-400 PSI	15-20 PSI
Sample consumption	10-20 μl/min	0.14-3.1 μl/min
Jet diameter	0.3-20 μm, typically 4-6 μm	1-10 μm jet, up to 50 μm in cone
Sample solvent	Water, lipidic cubic phase	30% glycerol/10% PEG 2000
V_{sample} for 30 min data collection	300 μl (50 μm ID)	5.1 μl (50 μm ID)
Sample delivery	Rotating syringe	Microcentrifuge tube
Operating pressure for SFX	$<3x10^{-5}$ Torr w/ diff. pumping	$1\text{-}7x10^{-5}$ Torr

*From [25] and references within

Supplementary References:

22. Jan Kern, Roberto Alonso-Mori, Julia Hellmich et al., *Proceedings of the National Academy of Sciences* **109** (25), 9721 (2012).
23. Hugh T. Philipp, Marianne Hromalik, Mark Tate et al., *Nuclear Instruments and Methods in Physics Research Section A: Accelerators, Spectrometers, Detectors and Associated Equipment* **649** (1), 67 (2011).
24. S. Boutet, L. Lomb, G. J. Williams et al., *Science* **337**, 362-364 (2012).
25. U. Weierstall, J. C. H. Spence, and R. B. Doak, *Review of Scientific Instruments* **83** (3), 035108 (2012).